Journal of proteome research

pubs.acs.org/jpr

Article

Identification of ALDH6A1 as a Potential Molecular Signature in Hepatocellular Carcinoma via Quantitative Profiling of the Mitochondrial Proteome

Heon Shin, Hyun-Jeong Cha, Min Jung Lee, Keun Na, Donha Park, Chae-Yeon Kim, Dai Hoon Han, Hoguen Kim, and Young-Ki Paik*

Cite This: *J. Proteome Res.* 2020, 19, 1684–1695

Read Online

ABSTRACT: Various liver diseases, including hepatocellular carcinoma (HCC), have been linked to mitochondrial dysfunction, reduction of reactive oxygen species (ROS), and elevation of nitric oxide (NO). In this study, we subjected the human liver mitochondrial proteome to extensive quantitative proteomic profiling analysis and molecular characterization to identify potential signatures indicative of cancer cell growth and progression. Sequential proteomic analysis identified 2452 mitochondrial proteins, of which 1464 and 2010 were classified as nontumor and tumor (HCC) mitochondrial proteins, respectively, with 1022 overlaps. Further metabolic mapping of the HCC mitochondrial proteins narrowed our biological characterization to four proteins, namely, ALDH4A1, LRPPRC, ATP5C1, and ALDH6A1. The latter protein, a mitochondrial methylmalonate semialdehyde dehydrogenase (ALDH6A1), was most strongly suppressed in HCC tumor regions (~10-fold decrease) in contrast to LRPPRC (~6-fold increase) and was predicted to be present in plasma. Accordingly, we selected ALDH6A1 for functional analysis and engineered Hep3B cells to overexpress this protein, called ALDH6A1-O/E cells. Since ALDH6A1 is predicted to be involved in mitochondrial respiration, we assessed changes in the levels of NO and ROS in the overexpressed cell lines. Surprisingly, in ALDH6A1-O/E cells, NO was decreased nearly 50% but ROS was increased at a similar level, while the former was restored by treatment with *S*-nitroso-*N*-acetyl-penicillamine. The lactate levels were also decreased relative to control cells. Propidium iodide and Rhodamine-123 staining suggested that the decrease in NO and increase in ROS in ALDH6A1-O/E cells could be caused by depolarization of the mitochondrial membrane potential ($\Delta\Psi$). Taken together, our results suggest that hepatic neoplastic transformation appears to suppress the expression of ALDH6A1, which is accompanied by a respective increase and decrease in NO and ROS in cancer cells. Given the close link between ALDH6A1 suppression and abnormal cancer cell growth, this protein may serve as a potential molecular signature or biomarker of hepatocarcinogenesis and treatment responses.

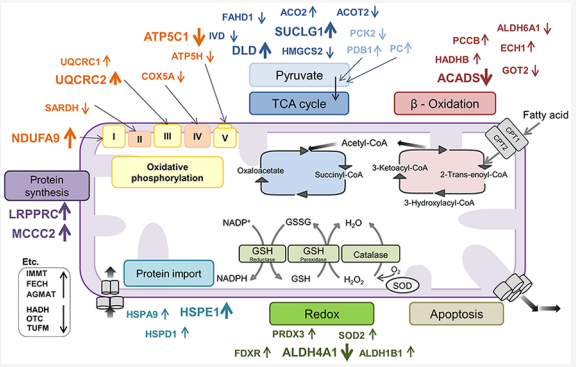

KEYWORDS: *ALDH6A1, hepatocellular carcinoma, mitochondria, nitric oxide, reactive oxygen species*

INTRODUCTION

Hepatocellular carcinoma (HCC) is among the most prevalent malignancies in Asian countries and the most rapidly increasing incidence in the United States, ranking the third leading cause of cancer-related death worldwide.[1] Globally, approximately 87% of HCC cases are associated with hepatitis C virus (HCV) and chronic hepatitis B virus (HBV) infections.[2] Many types of liver diseases, including HCC, are known to cause mitochondrial dysfunction.[3] This condition is associated with high levels of reactive oxygen species (ROS) production, particularly in HCC, alcoholic liver disease[4] and nonalcoholic fatty liver disease.[5]

The mitochondria play a central role in cellular energy homeostasis, metabolism, and cell death via the electron transport chain that synthesizes ATP in the inner membrane.[6] Consequently, the leakage of electrons induces the production of ROS, which contribute to cellular aging and DNA damage.[7] Mitochondrial dysfunction is also known to elevate nitric oxide (NO) levels in HCC cells.[8] In these cells, NO acts to suppress cellular respiration and enhance glycolysis,[9] which are typical phenomena in HCC cells.[10] Therefore, NO and ROS play very prominent roles in malignancies, wherein mitochondrial function and membrane potential appear to influence cancer cell growth and maintenance.

Received: December 12, 2019
Published: January 27, 2020

https://dx.doi.org/10.1021/acs.jproteome.9b00846
J. Proteome Res. 2020, 19, 1684–1695

Although some proteomic and molecular pathogenesis studies of HCC have evaluated the levels of various mitochondrial molecules,[11] the functional aspects of these molecules remain poorly understood in human HCC tumors. Therefore, we performed extensive quantitative proteomic profiling analyses of HCC tumors as well as Hep3B cell lines, and subsequent molecular characterization to identify any differentially expressed mitochondrial proteins in human HCC tissues. Here, we identified ALDH6A1 as a potential molecular signature, which reflects not only abnormal NO and ROS production but also mitochondrial respiratory function in HCC.

EXPERIMENTAL SECTION

Clinical Specimens

All clinical samples were obtained from the archives of the Department of Pathology, Yonsei University (Seoul, Korea), and the Liver Cancer Specimen Bank of the National Research Resource Bank Program affiliated with the Korea Research Foundation of the Ministry of Science and Technology. All diagnoses of HCC (n = 25) (Table S1, Supporting Information) were made by pathologists at Severance Hospital, Yonsei University. Twenty-five cases of HCC were included. The mean age (± standard deviation [SD]) and male: female ratio of each group was 54.6 ± 12.5 and 22:3, respectively. This research was approved by the Institutional Review Board (IRB, 4-2015-0474) of the Yonsei University College of Medicine.

Child-Pugh Classification

The severity of liver disease was assessed in each patient based on five clinical features: total bilirubin level, serum albumin, prothrombin time, the degree of ascites, and the grade of hepatic encephalopathy. The total point score was used to determine the patient's Child-Pugh class: Class A (a score of 5−6), Class B (7−9), or Class C (10 or above) (Table S1, Supporting Information). The Class B level has been accepted as a criterion for listing liver transplantation indicating, liver decompensation.

Sample Preparation for Proteomic Analysis

The tissue samples were washed with phosphate-buffered saline (PBS) solution and stored at −80 °C until use.[12] Tissue (100 mg) was homogenized in modified RIPA buffer (50 mM Tris−HCl, 150 mM NaCl, 1% NP-40, and 0.25% sodium deoxycholate, pH 7.4) containing a protease inhibitor (Sigma-Aldrich, St. Louis, MO), and the supernatant was collected via centrifugation at 14 000 rpm for 20 min. The protein concentration was determined using a 2D Quant kit (GE Healthcare, Uppsala, Sweden). After lysis, we concentrated and purified the cell lysates using Amicon Ultra centrifugal filters (Millipore, Billerica, MA). The human liver mitochondria standard was purchased from XenoTech (Lenexa, KS). The standard mitochondrial protein was only used for internal authenticity verification of the HCC tumor mitochondrial fraction by cross-comparison of protein bands between two samples in Western blot. The experiment was initiated with 50 μg of protein to minimize loss during the desalting process. The protein was diluted in 50 μL, and 1 μL of the solution was then injected into the liquid chromatography with tandem mass spectrometry (LC/MSMS). Therefore, the total amount of each peptide was 1 μg. The peptide samples from the in-solution digestion were desalted with an Oasis HLB column (Waters, Milford, MA) and lyophilized using a speed vac. Next, the peptides were dissolved in 0.1% formic acid and 3% acetonitrile (ACN) in a volume of 50 μL, and 1 μL was loaded onto a nano-LC-MS/MS.

Mitochondrial Enrichment

Differential centrifugation was used to enrich mitochondria in liver tissue samples (tumor or nontumor). After lysis of the liver tissue, the supernatant was centrifuged at 800g for 10 min. The pellet was discarded to remove the unbroken cells and nuclei. Next, the supernatant was centrifuged at 7000g for 15 min, and the supernatant was discarded. Next, the resulting pellet was transferred to a new tube and centrifuged at 18 000g for 25 min. The mitochondrial protein pellets were resuspended in 50 μL of liver mitochondria isolation buffer containing protease inhibitor.[13] The extent of mitochondrial enrichment was estimated by western blotting for the respective mitochondrial and cytosolic markers COX4 and β-actin.

Trypsin Digestion

Pelleted proteins from nontumor and tumor (HCC) tissue samples (50 μg/sample) were digested by in-solution. In-solution digestion was performed according to the modified protocol, as previously described.[14] The sample for denaturation and reduction was added to 8 M urea/5 mM DTT/25 mM NH_4HCO_3 (pH 8.0), and the tube was incubated at 60 °C for over 1 h. The resulting solution was cooled at room temperature. The solution was prepared at room temperature in 25 mM iodoacetamide in the dark for 20 min. Urea was diluted to a concentration of 1 M with 25 mM NH_4HCO_3 (pH 8.0) and then subjected to proteolytic digestion with trypsin (Promega Co., Madison, WI) at an enzyme to substrate ratio of 1:20 at 37 °C overnight. The peptide samples from the in-solution digestion were desalted with an Oasis HLB column (Waters, Milford, MA) and were lyophilized using a speed vac. Then, the dry residues were resuspended in 50 μL of loading buffer containing 0.1% formic acid and 3% ACN, and 1 μL was loaded onto nano-LC-MS/MS.

Large-Scale Tandem Mass Spectrometry (MS/MS) Data Collection and Analysis

Liquid chromatography separation was performed using an Ultimate 3000 RS nano-LC system (Thermo Scientific, MA). A C18 Easy nanocolumn (150 mm, 75 μm, 3 μm particle size, 100A pore size, Thermo) was used for peptide separation. The mobile phase A for the LC separation consisted of 0.1% formic acid in deionized water, and the mobile phase B consisted of 0.1% formic acid in acetonitrile. Then, 1 μg of desalted peptides was loaded onto the column with a starting mobile phase of 4% ACN and 0.1% formic acid. The chromatography gradient consisted of 2% ACN for 10 min with a linear increase from 4% B to 40% B over 55 min, 40% B to 60% B over 5 min, 95% B for 7 min, and 4% B for 11 min at a flow rate of 500 μL/min. Mass spectra were acquired with an Orbitrap Q Exactive mass spectrometer (Thermo Fisher, San Jose, CA) for the identification or quantification of peptides, with automatic switching between MS and MS/MS scans using a top-10 method. MS spectra were acquired at a resolution of 70 000 with an automatic gain control (AGC) target value of 1 × 106 ions or maximum integration time of 100 ms. The full MS scan ranges were acquired from 350 to 1800 m/z. The minimum threshold was set to 20 000 ion counts. Peptide fragmentation was performed via higher-energy collision dissociation (HCD)

https://dx.doi.org/10.1021/acs.jproteome.9b00846
J. Proteome Res. 2020, 19, 1684−1695

with the energy set at 27 NCE. Intensity threshold for ion selection was set at 1.0 e 5 with charge exclusion of $z = 1$ and $z > 7$. The MS/MS spectra were acquired at a resolution of 17 500, with a target value of 2 × 105 ions or maximum integration time of 120 ms, and the isolation window was set at 2.0 m/z. The mass spectrometry proteomics data have been interpreted according to HPP Guidelines[15] and deposited to the ProteomeXchange Consortium via the PRIDE partner repository with the data set identifier PXD014252.

Peptide Identification and Quantification

Proteome Discoverer software (version 1.4; Thermo Fisher Scientific) was used for protein identification and quantification. Mascot (version 2.1: Matrix Science) was used as a search engine. Peptides were identified using UniProt (release date: June 2012; www.uniprot.org). The database search criteria were as follows: taxonomy, Homo sapiens (86 875 sequences); carboxyamidomethylated (+57) at cysteine residues for fixed modifications; oxidized (+16) at methionine residues for variable modifications; maximum of two allowed missed cleavages; 10 ppm MS tolerance, a 0.1 Da CID, and 20 mmu (high-energy collision dissociation [HCD]) MS/MS tolerance. Only peptides resulting from tryptic digests were considered. For normalization and alignment of intensity and retention time, SIEVE 2.1 (Thermo Fisher Scientific, MA) was used according to the manufacturer's protocol. Here, "frames" represent rectangular regions in the m/z vs retention time plane, whereas "hits" refer to MS/MS identification scans. One can lower the threshold value and increase the number of frames if required. These settings produce more peaks and might produce more false positives.

Western Blot Analysis

Sample proteins were separated by 10% sodium dodecyl sulfate−polyacrylamide gel electrophoresis (SDS−PAGE) and transferred onto nitrocellulose membranes using an iBLOT dry blotting system (Invitrogen, Carlsbad, CA). The membranes were then blocked with TBS-T buffer (20 mM Tris, 137 mM NaCl, 0.1% Tween-20, 5% skim milk, pH 7.6), incubated overnight at 4 °C with anti-ALDH4A1, anti-APTG (ab119686), anti-COX4 (ab16056), anti-HSP60 (ab46798, abcam), anti-LRP130 (sc-66845), or anti-ALDH6A1 (sc-271582, SantaCruz) antibody, and subsequently incubated for 1 h with a 1:5000 dilution of secondary antibody (SantaCruz). Immunoreactive proteins were detected using ECL Plus Western blotting detection reagents (GE Healthcare, Chicago, IL). Western blot experiments were carried out using the biological replicates, as seen in Figure S1 (Supporting Information), in which uncropped membrane data were included.

Comparison of ALDH6A1 Expression in Various Tissues

ALDH6A1 was identified using GEPIA,[16] a tool that enables web server-based gene expression profiling interactive analysis based on the TCGA database. GEPIA measures gene expression levels in units of transcripts per million (TPM) and transformed into $\log_2$(TPM + 1) values. Next, the median expression in each cancer type was calculated to generate a bar plot of the *ALDH6A1* transcriptome abundance in TCGA and its normal counterpart tissues. Then, the median (expression value) of each tissue type was calculated to determine whether differences between the two samples were statistically significant. We determined whether differences between the two samples were statistically significant, differential analysis was performed using a one-way analysis of variance (ANOVA) and the $\log_2$ (fold change), defined as the median (tumor)−median (normal). *ALDH6A1* was searched in 32 cancer tissues using the TCGA Pan-Can Atlas[17] and cbioportal.[18] In each tissue, the *ALDH6A1* expression level was measured in TPM using the TCGA RNASeqV2 data and normalized using RSEM (RNA-Seq by expectation-maximization) to generate $\log_2$-scale plots of the *ALDH6A1* transcriptome abundance.

Preparation of ALDH6A1-O/E (Overexpression) Cell Lines

The Hep3B HCC cell line was purchased from ATCC (Manassas, VA). A Mycoprobe mycoplasma detection kit (R&D Systems, Minneapolis, MN) was used to identify the cell line as mycoplasma-negative. The following ATCC-specified cell culture media were used: Dulbecco's modified Eagle's medium (DMEM) supplemented with 10% fetal bovine serum and Hank's balanced salt solution (HBSS; Gibco, Grand Island, NY). The cells were cultured in a 37 °C incubator with an atmosphere of 5% CO_2. Hep3B cells were transfected (with the pCMV6-Entry vector with or without human ALDH6A1 cDNA) using Lipofectamine 3000 (Invitrogen) and selected using G418 (Sigma-Aldrich, St. Louis, MO) to isolate ALDH6A1-O/E cells according to the manufacturer's instructions. All of the cellular experiments were performed using stably transfected Hep3B cell lines. Human *ALDH6A1* and human *ATP5C1* DNA were purchased from Origene (Rockville, MD).

Measurement of Nitric Oxide (NO)

Hep3B cells and ALDH6A1-O/E cells were seeded into 6-well plates at the same density (0.8 × 10^5 cells/2 mL DMEM). The medium in each well was replaced with HBSS on the following day. The cells were then incubated with 5 μM 4-amino-5-(*N*-methylamino)-3′,6′-bis(acetyloxy)-2′7′difluoro-spiro-[isobenzofuran-1(3*H*), 9′-[9*H*]xanthen]-3-one (DAF-FM DA; Sigma-Aldrich) in a 37 °C incubator with a 5% CO_2 atmosphere for 20 min as described above. Additionally, the cells treated with 100 μM *S*-nitroso-*N*-acetyl-penicillamine (SNAP; Sigma-Aldrich, St. Louis, MO), a NO donor, were used as the positive control. The absorbance of each well at 488 nm was analyzed using a plate reader. The average absorbance is the value of NO levels.

Measurement of Reactive Oxygen Species (ROS)

Hep3B cells and ALDH6A1-O/E cells were seeded into 6-well plates at the same density (0.8 × 10^5 cells/2 mL DMEM). The medium in each well was replaced with HBSS on the following day. The cells were subsequently incubated with 10 μM DCF-DA (2′,7′-dichlorofluorescein diacetate; Sigma-Aldrich) in a 37 °C incubator with a 5% CO_2 atmosphere for 20 min as described above. The absorbance of each well at 488 nm was analyzed using a plate reader. The average absorbance is the value of ROS levels.

Mitochondrial Membrane Potential

Hep3B cells and ALDH6A1-O/E cells were seeded into 6-well plates at the same density (0.8 × 10^5 cells/2 mL DMEM). The medium was replaced with HBSS on the following day. Subsequently, the cells were incubated with 10 μg/mL Rhodamine-123 (Sigma-Aldrich) in a 37 °C incubator with a 5% CO_2 atmosphere for 8 min, and the absorbance of each well at 488 nm was analyzed using a plate reader at 30 sec intervals. FCCP (carbonyl cyanide 4-(trifluoromethoxy) phenylhydrazone) was used to disrupt the membrane. The average absorbance is the value of membrane potentials.

https://dx.doi.org/10.1021/acs.jproteome.9b00846
J. Proteome Res. 2020, 19, 1684−1695

Lactate Assay

Hep3B cells and ALDH6A1-O/E cells were seeded into 96-well plates at the same density (0.4×10^5 cells/100 μL DMEM). Cellular lactate levels were measured using an L-lactate assay kit (BioAssay Systems LLC, Hayward, CA) according to the manufacturer's instructions.

Propidium Iodide (PI) Staining

Hep3B cells and ALDH6A1-O/E cells were seeded into 6-well plates (0.8×10^5 cells/2 mL DMEM) and incubated with propidium iodide in an RNase staining buffer (BD Biosciences, San Jose, CA) for 30 min. The absorbance of each well at 493/636 nm was analyzed using a plate reader.

Statistical Analysis

All data are presented as means ± SDs. Three independent experiments (biological replicates) were performed per assay, and the data were analyzed using Student's *t*-test (technical replicates). A *p*-value of <0.05 was considered to indicate statistical significance.

RESULTS

Human Mitochondrial Protein Extraction

To identify specific mitochondrial protein(s) that might be involved in liver tumorigenesis (e.g., HCC), we prepared whole mitochondrial extracts of Edmondson grade II/III tumor and the adjacent nontumor samples from similarly aged male HCC patients (adjusted age: 50−59 years) (Figure S2A, Supporting Information) as outlined (Figure 1).[19] We further

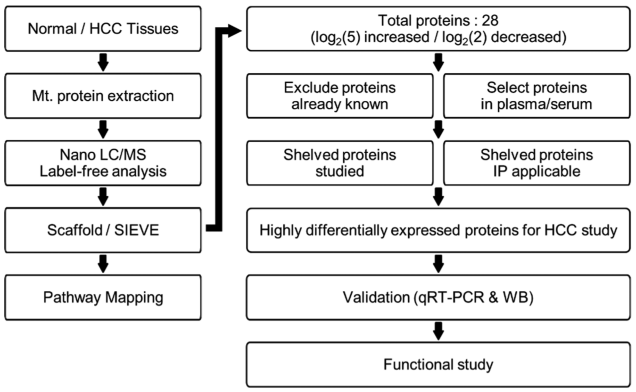

Figure 1. Schematic representation of the overall workflow.

fractionated the solubilized HCC tissue lysates using differential centrifugation to enable quantitative MS analysis of these mitochondrial proteins. Each lysate fraction was subjected to western blotting for the standard mitochondrial markers, COX4 and HSP60, to confirm the enrichment of mitochondrial proteins in the final sample fractions (Figure S2B, Supporting Information). Notably, the extracted mitochondria from HCC samples yielded essentially the same pattern of labeled protein bands as the commercial human mitochondria sample (Figure S2C, Supporting Information) (lane 1, labeled as "control" in the blot). We used this mitochondrial fraction for subsequent experiments unless otherwise specified.

Quantitative Proteomic Profiling and Gene Ontology (GO) Analysis of the HCC Mitochondrial Proteome

The relative expression levels of mitochondrial proteins were compared between the tumor and adjacent nontumor tissues from eight patients with HCC using a shotgun proteomic analysis facilitated by a high-resolution Q Exactive LC-MS spectrometer.[20] Our analysis resulted in the identification of 2452 proteins. The protein thresholds were 88.0% minimum (cut-off values) and a 2 peptide minimum, with a protein false discovery ratio (FDR) of 1.0% (decoy), and the peptide thresholds were 5.0% minimum (cut-off values) with a peptide FDR of 0.1% (decoy). They were largely classifiable into two groups: 1464 nontumor mitochondrial proteins and 2010 HCC mitochondrial proteins,[13,21] with 1022 proteins overlapping both groups (Figure S2D, Supporting Information). After excluding the latter 1022 proteins, 988 and 442 proteins from the tumor and nontumor regions remained, respectively (Figure S2D, Supporting Information, left panel). However, these numbers might have included proteins localized in both the mitochondria and cytosol.

For GO analysis, we selected 239 mitochondrial proteins that were well matched to annotated mitochondrial proteins deposited in the UniProt human protein database. These proteins included 194 proteins expressed in the tumor region and 188 expressed in the nontumor region (Figure S2D, Supporting Information, right panel), of which 143 were predicted to overlap between the regions. To further differentiate the gene sets encoding these mitochondrial proteins, the 239 differentially expressed mitochondrial proteins were subjected to GO analysis according to the molecular function, cellular component, and biological process (Figure S2E, Supporting Information). In the molecular functional group, proteins with catalytic activity accounted for 68%, and the remainder were classified as binding proteins, transporters, and others for 12, 12, and 8%. In the cellular component group, proteins associated with cellular compartments, organelle, membrane, and macromolecular complexes accounted for 37, 25, 25, and 13%, respectively. In the biological process group, proteins associated with the metabolic process accounted for 82%, whereas those associated with localization and others accounted for 14 and 4%, respectively (Figure S2E, Supporting Information).

Distribution of HCC Mitochondrial Proteins in Metabolic Pathways

Next, we subjected proteins detected in the tumor or nontumor tissues to a further quantitative classification based on their expression level. We used the SIEVE program[22] to perform peptide quantitative analysis of these proteins as described in the Experimental Section. Subsequently, we compared the MS intensity values between the tumor and nontumor region according to the retention time in a chromatogram (Figure S3A, Supporting Information). SIEVE uses Chromalign, a proprietary algorithm, to align the data. Chromalign evaluates the quality of the alignment between the samples by assigning a score. Alignments with scores above 0.75 are considered acceptable for further quantitative analysis. After excluding the samples with scores lower than 0.75, our data showed an average alignment score of 0.896, with the control (normal) and HCC groups clustering together. SIEVE allows the calculated peptide ratios between the samples to be filtered not only based on p values using Fisher's combined probability test but also based on variations in the MS peak intensities between the experimental replicates.[23] Next, we constructed a principal component analysis (PCA) plot based on the MS data. A subsequent analysis using SIEVE software revealed notable differences between principal components 1 and 2 (Figure S3B, Supporting Information). This result

https://dx.doi.org/10.1021/acs.jproteome.9b00846
J. Proteome Res. 2020, 19, 1684−1695

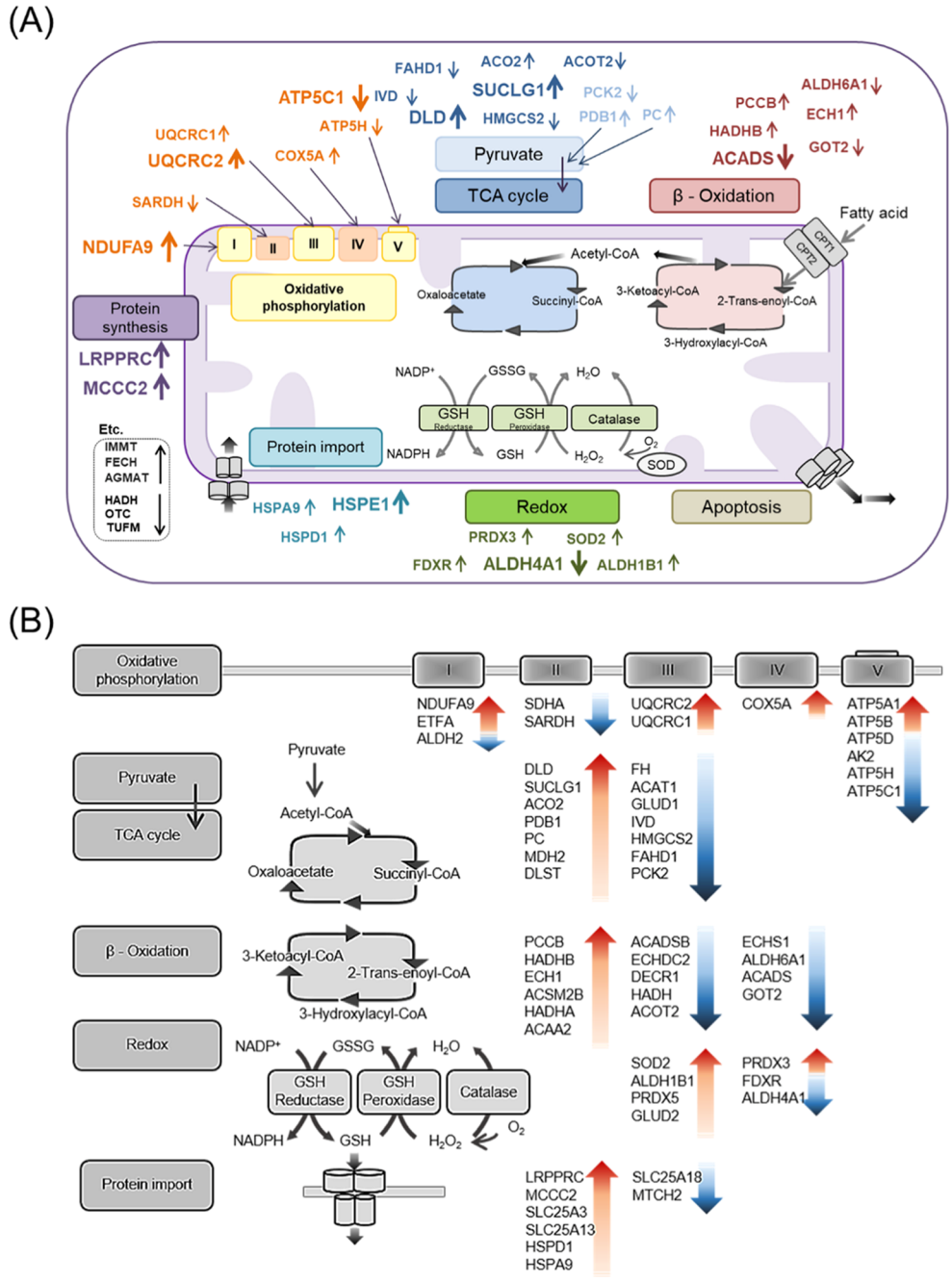

Figure 2. Map of mitochondrial proteomic interactions in hepatocellular carcinoma (HCC). (A) Differentially expressed peptides in mitochondrial protein samples from nontumor and HCC patients were mapped based on mitochondrial function.[26] This figure is based on the peptide levels. Much decreases are denoted largely, and the arrow is pointed downward. (B) Differentially expressed peptides were mapped based on the stages of mitochondrial respiration. The respiratory complexes are as follows: complex I, NADH reductase; complex II, succinate dehydrogenase; complex III, cytochrome *c* reductase; complex IV, cytochrome *o* oxidase; and complex V, ATP synthase.

suggests that at least two different classes of mitochondrial proteins are present between tumor and nontumor regions.

Next, we attempted to map the differentially expressed proteins in HCC against a metabolic network, as this may inform our interpretation and understanding of the changes in individual mitochondrial proteins in the tumor and nontumor regions of HCC tissues. In an analysis focused on overall mitochondrial function (Figure 2A) and the oxidative respiratory pathway (Figure 2B), proteins with >2-fold differences between tumor and nontumor regions (i.e., upregulation, ↑) were mostly located in oxidative phosphorylation systems (except for Oxphos II) and tricarboxylic acid (TCA) cycle pathways (metabolic component supply) (Figure 2). This finding is consistent with a previous report, that is, regulation of mitochondrial energy metabolism and its interaction with cytoplasmic and other compartments.[24] Furthermore, it implies that the expression of a wide range of metabolic proteins during liver tumorigenesis is influenced by mitochondrial energy production pathways.

We next compared these findings with the database of differentially expressed proteins in human cancer (dbDEPC 3.0) (HCC Proteins-Heatmap)[25] and identified relatively high

https://dx.doi.org/10.1021/acs.jproteome.9b00846
J. Proteome Res. 2020, 19, 1684−1695

Table 1. Eight Candidate Mitochondrial Proteins Studied in Hepatocellular Carcinoma

no.	gene name	full name	possible function
1	ALDH4A1	delta-1-pyrroline-5-carboxylate dehydrogenase	interconnecting the urea and TCA cycle
2	LRPPRC	leucine-rich PPR motif-containing protein	RNA metabolism
3	ATP5C1	ATP synthase subunit γ	F_1F_0 ATP synthase
4	MCCC2	methylcrotonoyl CoA carboxylase β chain	leucine and isovaleric acid catabolism
5	SUCLG1	succinyl-CoA ligase, subunit α	catalyze the ATP-, GTP-dependent ligation of succinate and CoA to form succinyl-CoA
6	NDUFA9	NADH dehydrogenase 1 α subcomplex, subunit 9	transfer of electrons from NADH to the respiratory chain
7	ALDH6A1	methylmalonate semialdehyde dehydrogenase	valine and pyrimidine metabolism
8	ACOT2	acyl-coenzyme A thioesterase 2	catalyze the hydrolysis of acyl-CoAs to free fatty acid and CoASH

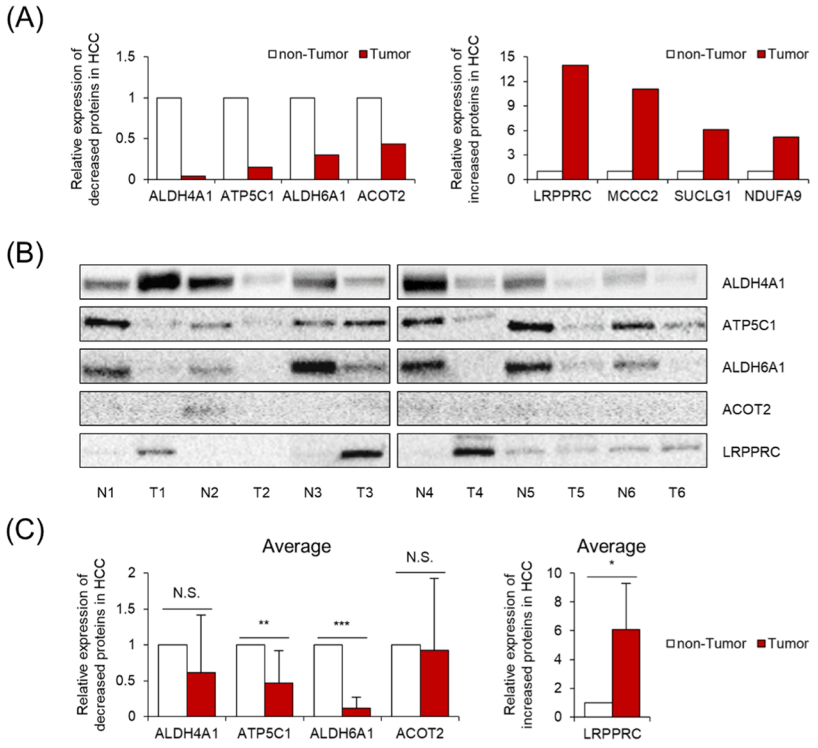

Figure 3. Expression levels of detected mitochondrial peptides and proteins. (A) Peptide levels of various proteins were determined by liquid chromatography (LC)-tandem mass spectrometry (MS/MS) and compared between nontumor and HCC tissues. (B) Protein levels in individual HCC patients were determined by western blotting. (C) Protein levels in individual samples from HCC patients were determined by western blotting. *p < 0.001, **p < 0.005, ***p < 0.0001. N.S., not significant for the indicated comparison.

similarities in the differential expression of these mitochondrial proteins in cells and tissues. However, we also observed some differences. For example, the peptide levels of several proteins (e.g., ETFA, ATP5A1, SUCLG1, PC, ECH1, ACSM2B, HADHA, ACAA2, PRDX3, and SLC25A13) are decreased in HCC according to the dbDEPC database but were increased in our data sets. The reverse pattern was observed for other proteins (e.g., ATP5D and FXDR). Moreover, some proteins (e.g., ATP5B, SOD2, ALDH1B1, and SLC25A3) that did not differ between tumor and nontumor regions in the dbDEPC were differentially expressed in our data set. Notably, we also identified some proteins not listed in the dbDEPC (e.g., PDB1, GLUD2, LRPPRC, MCCC2, ATP5C1, FADH1, ACOT2, and SLC25A18). The proteins with increased expression in tumor regions are involved in the TCA cycle, Huntington's disease, the degradation of branched amino acids (valine, leucine, and isoleucine), Alzheimer's disease, and Parkinson's disease pathways, whereas those with decreased expression in tumor regions are associated with the degradation of branched amino acids, fatty acid degradation, and butanoate and pyruvate metabolism.

Functional Prediction of Differentially Expressed Mitochondrial Proteins in HCC Tissues

We next selected 52 of 70 secreted mitochondrial proteins predicted by UniProt DB in HCC patients to identify a potential molecular signature of malignancy. Of the 28 differentially expressed proteins exhibiting either a $\log_2(5)$-fold increase or $\log_2(2)$-fold decrease in the plasma of HCC patients compared with nontumor patients, we selected eight mitochondrial proteins that were uniquely detected in HCC plasma via western blotting with a commercially available monoclonal antibody (mAb) (Table 1). A peptide-level MS analysis identified four proteins that were differentially expressed at the protein level (western blotting): ALDH4A1 (delta-1-pyrroline-5-carboxylate dehydrogenase), LRPPRC (a leucine-rich PPR motif-containing protein), ATP5C1 (ATP synthase subunit γ), and ALDH6A1 (methylmalonate semialdehyde dehydrogenase). MS revealed that LRPPRC, ATP5C1, and ALDH6A1 differed quantitatively between the

https://dx.doi.org/10.1021/acs.jproteome.9b00846
J. Proteome Res. 2020, 19, 1684−1695

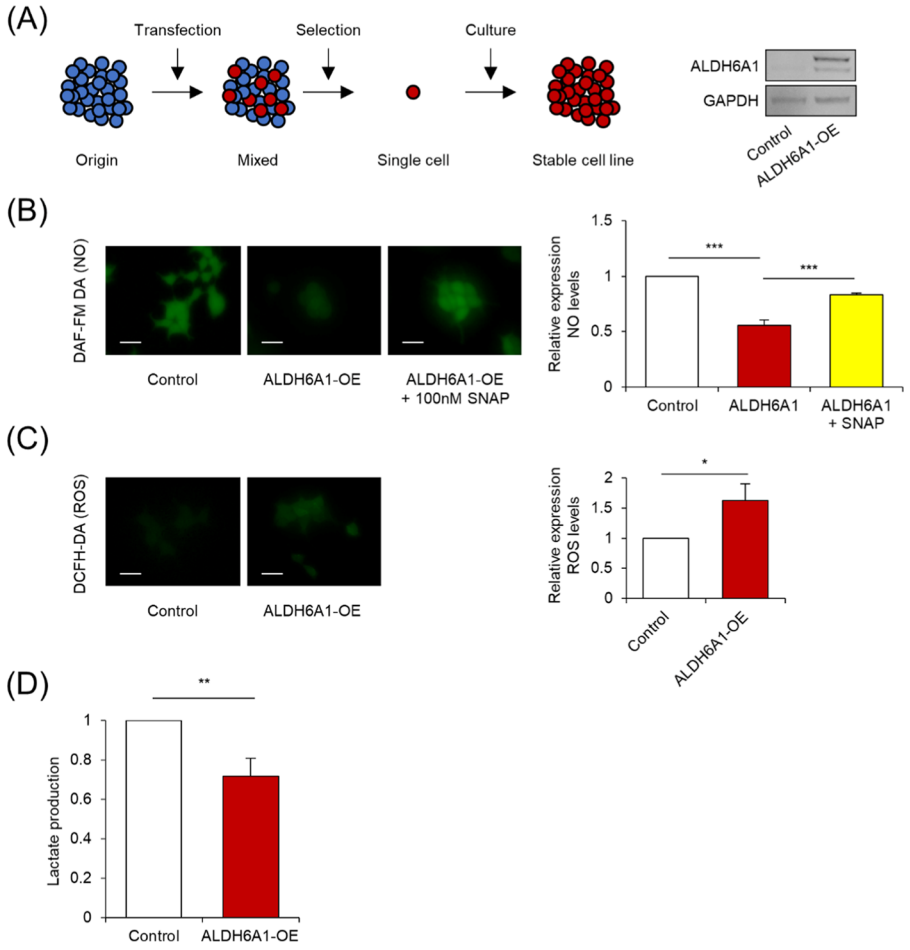

Figure 4. Establishment of an ALDH6A1-overexpressing cell line (ALDH6A1-OE) and measurement of reactive chemical species. (A) Schema of the establishment of ALDH6A1-overexpressing cell lines. Western blot analysis confirmed the successful overexpression of ALDH6A1. (B) Fluorescence imaging of nitric oxide (NO) in Hep3B cells and ALDH6A1-OE cells after adding a NO donor (SNAP), DAF-FM DA. The intensities of experimental samples were normalized to that of the control. (C) Fluorescence imaging of reactive oxygen species (ROS) in Hep3B cells and ALDH6A1-OE cells using DCFH-DA. The intensities of experimental samples were normalized to that of the control. (D) Lactate production in Hep3B cells and ALDH6A1-OE cells were detected using a lactate assay kit. The intensities of experimental samples were normalized to that of the control. $*p < 0.001$, $**p < 0.005$, and $***p < 0.0001$.

tumor and nontumor regions of HCC samples (Figure 3A). Specifically, a comparison of tumor relative to nontumor expression yielded a maximum increase of 14-fold and 6.1-fold in the LRPPRC peptide and protein, a 6-fold and 2.1-fold decrease in the ATP5C1 peptide and protein, and a 3.3-fold and 8.4-fold decrease in the ALDH6A1 peptide and protein levels, respectively (Figures 3A,B and S4, Supporting Information). Western blot analyses of individual HCC tissue samples revealed an approximately 6-fold increase in LRPPRC and an ∼10-fold and 2-fold decrease in ALDH6A1 and ATP5C1, respectively (Figure 3C). In contrast, the levels of ALDH4A1 did not differ significantly between the tumor and nontumor regions. As LRPPRC was previously studied as a potential biomarker for colorectal cancer[27] and ATP5C1 is a common enzyme in energy metabolism,[28] ALDH6A1 was selected for further functional analyses.

Negative Correlation between NO Levels and ALDH6A1 Expression in HCC

We next explored why ALDH6A1 was expressed at high levels in nontumor regions but suppressed in HCC tumor regions (Figures 3 and S5A, Supporting Information). To characterize the potential cellular or regulatory function of ALDH6A1 with respect to hepatocellular carcinogenesis, we engineered Hep3B cells, which express low levels of endogenous ALDH6A1, to overexpress this protein (ALDH6A1-O/E cells) (Figure 4A). ALDH6A1, one of the human ALDH super families, is usually involved in mitochondrial respiration, which is highly influenced by the changes in NO and ROS levels.[29] First, we wanted to assess changes in NO and ROS levels in ALDH6A1-O/E cells. Surprisingly, we detected a fairly low level of NO in ALDH6A1-O/E cells (Figure 4B), which is quite opposite to that in Hep3B cells. This lower level of NO was recovered to approximately 78% of the control when the ALDH6A1-O/E cells were treated with *S*-nitroso-*N*-acetyl-penicillamine (SNAP), a nitrosothiol derivative that releases NO under certain physiological conditions (Figure 4B). Second, since an opposite relation has been identified between NO and ROS in Hep3B cells as well as ALDH6A1-O/E cells, we then checked ROS levels in the overexpressed cells. We found that the ROS levels were increased by approximately 50% ALDH6A1-O/E cells relative to the control cells (Figure 4C). Additionally, ALDH6A1-O/E cells exhibited a decreased level of lactate (Figure 4D), consistent with previous studies of hepatoma cell lines.[32] Taken together, these data suggest that NO levels are negatively correlated to the expression of mitochondrial

https://dx.doi.org/10.1021/acs.jproteome.9b00846
J. Proteome Res. 2020, 19, 1684−1695

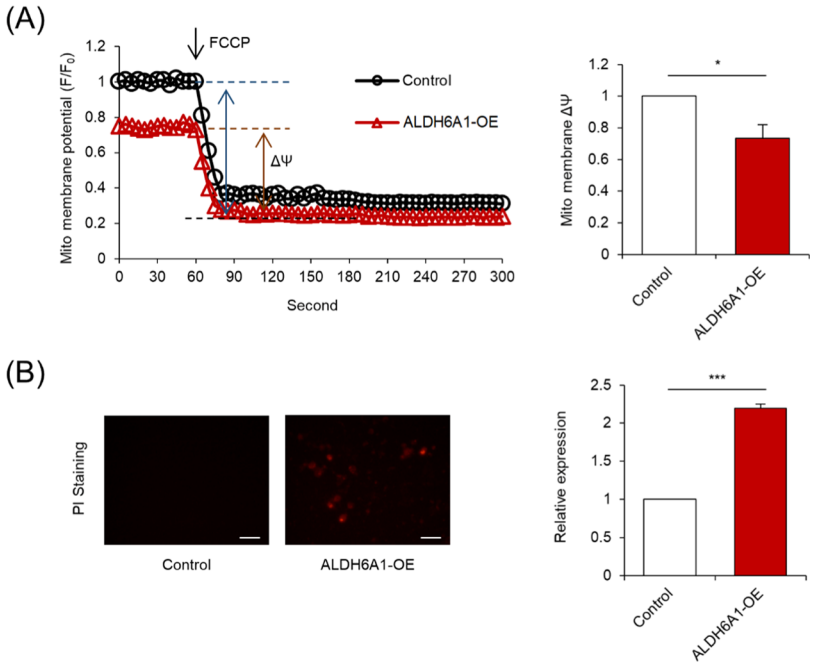

Figure 5. Variations in mitochondrial membrane potential and cell death. (A) Mitochondrial membrane potential (ΔΨ) values are normalized to that of the control. (B) Fluorescence imaging of cell death in propidium iodide-stained Hep3B cells and ALDH6A1-OE cells. The intensities were normalized to that of the control. *p < 0.001 and ***p < 0.0001.

ALDH6A1 in HCC. This supports the notion that ALDH6A1 may play a role as a signatory or biomarker molecule in liver cancer. This deserves further validation work using the HCC patients' plasma samples.

Role of ALDH6A1 in the Maintenance of Mitochondrial Membrane Potential in HCC

In some cancer cells, a low level of NO is coupled with a depolarized membrane potential (ΔΨ), and these features have been linked to uncontrolled proliferation and differentiation.[33] However, the underlying mechanisms are not fully characterized. To clarify the mechanism underlying the opposite patterns of NO and ROS production in ALDH6A1-O/E cancer cells, we measured the membrane potential in these and control cells. As expected, we observed a depolarized mitochondrial membrane potential (ΔΨ) in ALDH6A1-O/E cells (Figure 5A), and PI staining suggested that this depolarization might have caused cell death (Figure 5B). We tentatively suggest that in cancer cells ALDH6A1 expression is strongly suppressed, which may subsequently promote uncontrolled cell growth and proliferation (Figure 6).[34,35]

DISCUSSION

The most important step in this study was the validation of our enriched mitochondrial protein samples using mitochondrial marker proteins (e.g., COX4 and HSP60) and β-actin (dual-localization in the cytosol and mitochondria) (Figure S2C, Supporting Information).[36] This efficient enrichment, together with a highly stringent cut-off (peptide level, < 1% FDR), enabled us to detect >2500 mitochondrial proteins, one of the largest populations identified using shotgun proteome profiling to date.[37] The achievement of a highly enriched mitochondrial fraction is one of the most difficult steps in a mitochondrial protein study.[38] Therefore, we hope that our data may contribute to existing data sets of mitochondrial proteins.[39]

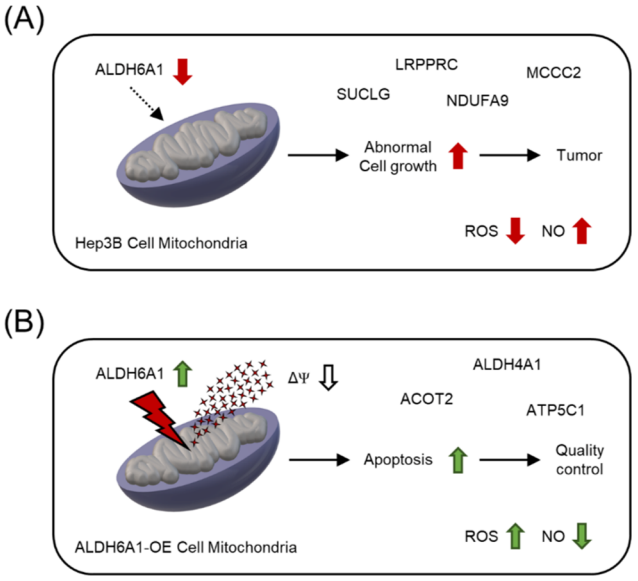

Figure 6. Proposed role for ALDH6A1 in hepatocellular carcinogenesis. (A) Levels of ALDH6A1 were found to be very low in HCC cells. This phenomenon is accompanied by a decreased level of ROS and increased levels of NO, which may support abnormal tumor cell growth. Proteomic analysis also identified increased levels of LRPPRC, SUCLG, MCCC2, and NDRFA9 in HCC cells. (B) When the levels of ALDH6A1 were increased in its overexpression cells (ALDH6A1-O/E), ROS is increased, but NO is decreased, which results in the stimulation of apoptosis. Proteomic analysis also identified increased levels of ALDH4A1, ACOT2, and ATP5C1 in ALDH6A1-O/E cells.

Notably, our GO analysis-based comparison of mitochondrial proteins in HCC tissues revealed that in the molecular function field, a reduction of approximately 4% in the number of proteins attributed to catalytic activity was observed in

https://dx.doi.org/10.1021/acs.jproteome.9b00846
J. Proteome Res. 2020, 19, 1684−1695

tumor regions relative to the number in nontumor regions. Proteins associated with cellular component organization or biogenesis accounted for approximately 3.1% of those in the biological process field. The proteins identified in the tumor regions of HCC included dynamin-like 120 kDa protein, mitochondrial import inner membrane translocase 9 (TIM9), and TIM44, which are involved in apoptosis and mitochondrial fusion. Overall, the observed reductions in proteins associated with metabolism were consistent with a previous report.[40] Taken together, these results suggest that reduced ATP production and signal transduction are typical phenomena in cancer cells.[41]

Moreover, our data clearly demonstrate the upregulation of LRPPRC, SOD2, and UQCRC1 and 2 expression in mitochondria from the tumor region. These proteins are involved in antiapoptotic processes, tumorigenesis, and uncontrolled cell growth.[42] Interestingly, we also observed the downregulation of ornithine transcarbamylase (OTC), a liver-specific mitochondrial matrix enzyme involved in liver fibrosis and biomarker of HCC.[43] This finding was consistent with previous studies of hepatitis B and C patients.[44] In particular, we observed a very high level of LRPPRC expression in the tumor regions of HCC, again consistent with a previous report that identified this protein as an antiapoptotic and tumorigenic marker.[45]

Based on our previous works where alternation of ALDH isozyme variants was found to be closely correlated to HCC,[46] we proposed that like other ALDH isozymes, ALDH6A1 may also have a role of molecular signature to indicate progress on cancer cell growth. This proposal can be supported in part that ALDH6A1 was identified as one of six genes associated with the risk and prognosis of HCC metastasis.[45] Even more, our results on the ALDH6A1 are consistent with those of Jiang et al. (CNHPP liver data set).[47] As outlined in Figure 6, ALDH6A1 expression seems to have a negative correlation with cancer progression,[34,35,45,48] although the underlying mechanism has not been explored. After completing our proteomic analysis, we cross-checked public genomic databases to identify molecular evidence of ALDH6A1 expression in various cancers. We found that in a normal state, liver tissues expressed substantially higher levels of *ALDH6A1* than tumor state (Figure S5A, Supporting Information). Similarly, nearly all surveyed cancer tissues exhibited lower ALDH6A1 levels relative to normal tissues (Figure S5B, Supporting Information). It was also noted that HCC exhibited a relatively higher expression level of ALDH6A1 compared to other cancer tissues surveyed (Figure S5C, Supporting Information). Interestingly, ALDH6A1 expression decreases with cellular aging,[49] suggesting that this protein also plays important roles in cellular metabolism and cancer cell progression. Notably, the lack of ALDH6A1 appears to be associated with developmental delays.[50] In addition, based on its KEGG pathway description (a database designed to evaluate the high-level functions and utilities of biological systems) and its GO annotation, ALDH6A1 is also associated with propanoate metabolism, metabolic pathways, inositol phosphate metabolism, β-alanine metabolism, and carbon metabolism, as well as the valine, leucine, and isoleucine degradation pathways.

In HCC, the increased NO and the decreased ROS might have caused the host redox status. Although both are known to act together to induce cell death,[30,31] the former is expressed primarily in macrophages following exposure to cytokines and microbial products, whereas the latter is produced as a byproduct of stress and respiration. They are known to play dual roles with respect to tumor cell apoptosis during cancer progression,[51] and hence elevation of NO levels and reduction of ROS levels in HCC cells could be a target for cancer treatment. For example, overexpression of ALDH6A1 was clearly associated with cell death (Figure 5B), which appears to be due to depolarization of the mitochondrial membrane potential, leading to an increase in ROS and decrease in NO (Figure 6B), consistent with a previous report.[29] From the mechanistic point of view, it was previously reported that an increase in ALDH might induce a decrease in NAD+/NADH, which would then induce mitochondrial dysfunction and oxidative stress.[30] Considering this notion, we may propose that an increase in ALDH6A1 in ALDH6A1-O/E cells would cause a reduction in NAD+/NADH that consequently disrupts mitochondrial membrane potential (Figure 5A,B). The disruption in membrane potential would then lead to decreased NO and increased ROS levels. It is also conceivable that some parts of the increased ROS might react with NO, resulting in the production of peroxynitrite ($ONOO^-$), which may scavenge NO, leading to the decreased NO level (Figure 6B) as previously reported.[52] Even more, as the ROS level increases, some of these peroxynitrites would cause endothelial dysfunction.[53]

In conclusion, hepatic neoplastic transformation appears to suppress the expression of ALDH6A1, accompanied by a respective increase and decrease in NO and ROS (Figure 6A). Our findings may contribute to a better understanding of the progressive liver disease and could provide clues for the diagnosis and the response to treatment of HCC, provided the detection of plasma ALDH6A1 would be made by its antibody. Since ALDH6A1 is predicted to be present in both the mitochondria and plasma (UniProt, www.uniprot.org), it may be feasible to use anti-ALDH6A1 antibody for diagnostic purpose as in the case of hCE1, which showed very low expression in HCC tissue but higher expression in HCC plasma.[54] Given the close link between ALDH6A1 suppression and abnormal cancer cell growth, it deserves further study to examine if this protein would serve as a potential molecular signature or biomarker of hepatocarcinogenesis (in tissues or serum) and treatment responses.

■ ASSOCIATED CONTENT

Supporting Information

The Supporting Information is available free of charge at https://pubs.acs.org/doi/10.1021/acs.jproteome.9b00846.

Detailed information of 25 cases of HCC patients (XLSX)

Uncropped whole membrane images of western blot (Figure S1); clinicopathological data of patients with hepatocellular carcinoma (HCC) and the results of mitochondrial isolation and liquid chromatography (LC)-tandem mass spectrometry (MS/MS) analysis (Figure S2); quantitative analysis of mitochondrial proteins in hepatocellular carcinoma (HCC) based on the SIEVE program (Figure S3); protein levels in pooled HCC patients were determined by western blotting (Figure S4); comparison of *ALDH6A1* expression in various tumor tissues vs normal tissues (Figure S5); detailed information of 25 cases of HCC patients (Table S1); list of increased mitochondrial proteins (Table S2); list of decreased mitochondrial proteins (Table S3); list

https://dx.doi.org/10.1021/acs.jproteome.9b00846
J. Proteome Res. 2020, 19, 1684−1695

of total mitochondrial proteins (nontumor region) (Table S4); list of total mitochondrial proteins (tumor region) (Table S5); abbreviations for Supporting information Figure S4 (Table S6) (PDF)

AUTHOR INFORMATION

Corresponding Author

Young-Ki Paik − *Yonsei Proteome Research Center, Yonsei University, Seoul 03722, Republic of Korea;* orcid.org/0000-0002-8146-1751; Phone: +82-2-2123-4242; Email: paikyk@gmail.com; Fax: +82-2-393-6589

Authors

Heon Shin − *Yonsei Proteome Research Center, Yonsei University, Seoul 03722, Republic of Korea;* orcid.org/0000-0001-5480-8492

Hyun-Jeong Cha − *Yonsei Proteome Research Center, Yonsei University, Seoul 03722, Republic of Korea;* orcid.org/0000-0002-7426-9155

Min Jung Lee − *Yonsei Proteome Research Center, Yonsei University, Seoul 03722, Republic of Korea*

Keun Na − *Yonsei Proteome Research Center, Yonsei University, Seoul 03722, Republic of Korea*

Donha Park − *Yonsei Proteome Research Center, Yonsei University, Seoul 03722, Republic of Korea*

Chae-Yeon Kim − *Yonsei Proteome Research Center and Interdisciplinary Program of Integrated OMICS for Biomedical Science, Graduate School, Yonsei University, Seoul 03722, Republic of Korea*

Dai Hoon Han − *Department of Surgery and Department of Pathology, Yonsei University College of Medicine, Seoul 03722, Republic of Korea; Department of Pathology, College of Medicine, Severance Hospital, Yonsei University, Seoul 03722, Republic of Korea*

Hoguen Kim − *Department of Pathology, College of Medicine, Severance Hospital, Yonsei University, Seoul 03722, Republic of Korea*

Complete contact information is available at: https://pubs.acs.org/10.1021/acs.jproteome.9b00846

Author Contributions

Y.-K.P., H.S., and H.-J.C. designed the study; H.S. and H.-J.C. performed the research; H.K. and D.H.H. provided hepatocellular carcinoma samples and related scientific inputs; M.J.L., K.N., D.P., and C.-Y.K. analyzed data; Y.-K.P., H.S., and H.-J.C. wrote the paper.

Notes

The authors declare no competing financial interest.

Mass spectrometry data are available via ProteomeXchange with identifier PXD014252.

ACKNOWLEDGMENTS

This work was supported by grants from the Korean Ministry of Health and Welfare (HI160274 to Y.-K.P.), the Liver Cancer Specimen Bank funded by the National Research Foundation (2015M3A9B8028339 to H.K.), the Faculty Research Grant of Yonsei University College of Medicine (6-2016-0122 to D.H.H.), and a Severance Surgeon's Alumni Research Grant (2016-02 to D.H.H.). We thank the staff members of the Yonsei Proteome Research Center for their assistance with this project. We also thank the Severance Hospital Gene Bank for kindly supplying the tumor tissues and materials used in this work.

ABBREVIATIONS USED

ACOT2, acyl-CoA thioesterase 2; ALDH4A1, delta-1-pyrroline-5-carboxylate dehydrogenase; ALDH6A1, methylmalonate semialdehyde dehydrogenase; ATP5C1, ATP synthase subunit γ; HCC, hepatocellular carcinoma; LC-MS, liquid chromatography-mass spectrometry; LRPPRC, leucine-rich PPR motif-containing protein; MCCC2, methylcrotonoyl-CoA Carboxylase 2; NDUFA9, NADH:ubiquinone oxidoreductase subunit A9; NO, nitric oxide; TCGA, the cancer genome atlas; ROS, reactive oxygen species; SUCLG, succinyl-CoA ligase

REFERENCES

(1) Bray, F.; Ferlay, J.; Soerjomataram, I.; Siegel, R. L.; Torre, L. A.; Jemal, A. Global cancer statistics 2018: GLOBOCAN estimates of incidence and mortality worldwide for 36 cancers in 185 countries. *CA-Cancer J. Clin.* **2018**, *68*, 394−424.

(2) Abou-Alfa, G. K.; Jarnagin, W.; Dika, I. E.; D'Angelica, M.; Lowery, M.; Brown, M. Liver and Bile Duct Cancer. In *Abeloff's Clinical Oncology*, 6th ed.; Niederhuber, J. E.; Armitage, J. O.; Doroshow, J. H.; Kastan, M. B.; Tepper, J. E., Eds.; Elsevier: Philadelphia, Pa, 2020; pp 1314−1341.

(3) Lin, M. T.; Beal, M. F. Mitochondrial dysfunction and oxidative stress in neurodegenerative diseases. *Nature* **2006**, *443*, 787−795.

(4) Dasarathy, S. Nutrition and Alcoholic Liver Disease: Effects of Alcoholism on Nutrition, Effects of Nutrition on Alcoholic Liver Disease, and Nutritional Therapies for Alcoholic Liver Disease. *Clin. Liver Dis.* **2016**, *20*, 535−550.

(5) Brunt, E. M.; Wong, V. W.; Nobili, V.; Day, C. P.; Sookoian, S.; Maher, J. J.; Bugianesi, E.; Sirlin, C. B.; Neuschwander-Tetri, B. A.; Rinella, M. E. Nonalcoholic fatty liver disease. *Nat. Rev. Dis. Primers* **2015**, *1*, No. 15080.

(6) Bratic, I.; Trifunovic, A. Mitochondrial energy metabolism and ageing. *Biochim. Biophys. Acta* **2010**, *1797*, 961−967.

(7) Zorov, D. B.; Juhaszova, M.; Sollott, S. J. Mitochondrial reactive oxygen species (ROS) and ROS-induced ROS release. *Physiol. Rev.* **2014**, *94*, 909−950.

(8) Iwakiri, Y.; Kim, M. Y. Nitric oxide in liver diseases. *Trends Pharmacol. Sci.* **2015**, *36*, 524−536.

(9) Brown, G. C.; Borutaite, V. Nitric oxide and mitochondrial respiration in the heart. *Cardiovasc. Res.* **2007**, *75*, 283−290.

(10) Chang, C. F.; Diers, A. R.; Hogg, N. Cancer cell metabolism and the modulating effects of nitric oxide. *Free Radic. Biol. Med.* **2015**, *79*, 324−336.

(11) Ye, Y.; Huang, A.; Huang, C.; Liu, J.; Wang, B.; Lin, K.; Chen, Q.; Zeng, Y.; Chen, H.; Tao, X.; Wei, G.; Wu, Y. Comparative mitochondrial proteomic analysis of hepatocellular carcinoma from patients. *Proteomics: Clin. Appl.* **2013**, *7*, 403−415.

(12) Na, K.; Shin, H.; Cho, J. Y.; Jung, S. H.; Lim, J.; Lim, J. S.; Kim, E. A.; Kim, H. S.; Kang, A. R.; Kim, J. H.; Shin, J. M.; Jeong, S. K.; Kim, C. Y.; Park, J. Y.; Chung, H. M.; Omenn, G. S.; Hancock, W. S.; Paik, Y. K. Systematic Proteogenomic Approach To Exploring a Novel Function for NHERF1 in Human Reproductive Disorder: Lessons for Exploring Missing Proteins. *J. Proteome Res.* **2017**, *16*, 4455−4467.

(13) Alberio, T.; Pieroni, L.; Ronci, M.; Banfi, C.; Bongarzone, I.; Bottoni, P.; Brioschi, M.; Caterino, M.; Chinello, C.; Cormio, A.; Cozzolino, F.; Cunsolo, V.; Fontana, S.; Garavaglia, B.; Giusti, L.; Greco, V.; Lucacchini, A.; Maffioli, E.; Magni, F.; Monteleone, F.; Monti, M.; Monti, V.; Musicco, C.; Petrosillo, G.; Porcelli, V.; Saletti, R.; Scatena, R.; Soggiu, A.; Tedeschi, G.; Zilocchi, M.; Roncada, P.; Urbani, A.; Fasano, M. Toward the Standardization of Mitochondrial Proteomics: The Italian Mitochondrial Human Proteome Project Initiative. *J. Proteome Res.* **2017**, *16*, 4319−4329.

(14) Lee, H. J.; Kang, M. J.; Lee, E. Y.; Cho, S. Y.; Kim, H.; Paik, Y. K. Application of a peptide-based PF2D platform for quantitative

proteomics in disease biomarker discovery. *Proteomics* **2008**, *8*, 3371−3381.
(15) Deutsch, E. W.; Overall, C. M.; Van Eyk, J. E.; Baker, M. S.; Paik, Y. K.; Weintraub, S. T.; Lane, L.; Martens, L.; Vandenbrouck, Y.; Kusebauch, U.; Hancock, W. S.; Hermjakob, H.; Aebersold, R.; Moritz, R. L.; Omenn, G. S. Human Proteome Project Mass Spectrometry Data Interpretation Guidelines 2.1. *J. Proteome Res.* **2016**, *15*, 3961−3970.
(16) Tang, Z.; Li, C.; Kang, B.; Gao, G.; Li, C.; Zhang, Z. GEPIA: a web server for cancer and normal gene expression profiling and interactive analyses. *Nucleic Acids Res.* **2017**, *45*, W98−W102.
(17) Cancer Genome Atlas Research Network; Weinstein, J. N.; Collisson, E. A.; Mills, G. B.; Shaw, K. R.; Ozenberger, B. A.; Ellrott, K.; Shmulevich, I.; Sander, C.; Stuart, J. M. The Cancer Genome Atlas Pan-Cancer analysis project. *Nat. Genet.* **2013**, *45*, 1113−1120.
(18) Gao, J.; Aksoy, B. A.; Dogrusoz, U.; Dresdner, G.; Gross, B.; Sumer, S. O.; Sun, Y.; Jacobsen, A.; Sinha, R.; Larsson, E.; Cerami, E.; Sander, C.; Schultz, N. Integrative analysis of complex cancer genomics and clinical profiles using the cBioPortal. *Sci. Signaling* **2013**, *6*, pl1.
(19) Bassullu, N.; Turkmen, I.; Yaprak, O.; Dayangac, M.; Demirbas, T.; Guler, N.; Uraz, S.; Akyildiz, M.; Cigerciogullari, E.; Tokat, Y.; Yuzer, Y.; Dogusoy, G. B. General evaluation of hepatectomy and hepatocellular carcinoma cases. *Turk Patoloji Derg.* **2011**, *27*, 221−229.
(20) Shin, H.; Cha, H. J.; Na, K.; Lee, M. J.; Cho, J. Y.; Kim, C. Y.; Kim, E. K.; Kang, C. M.; Kim, H.; Paik, Y. K. O-GlcNAcylation of the Tumor Suppressor FOXO3 Triggers Aberrant Cancer Cell Growth. *Cancer Res.* **2018**, *78*, 1214−1224.
(21) Ronci, M.; Pieroni, L.; Greco, V.; Scotti, L.; Marini, F.; Carregari, V. C.; Cunsolo, V.; Foti, S.; Aceto, A.; Urbani, A. Sequential Fractionation Strategy Identifies Three Missing Proteins in the Mitochondrial Proteome of Commonly Used Cell Lines. *J. Proteome Res.* **2018**, *17*, 4307−4314.
(22) Slotta, D. J.; McFarland, M. A.; Markey, S. P. MassSieve: panning MS/MS peptide data for proteins. *Proteomics* **2010**, *10*, 3035−3039.
(23) Cholewa, B. D.; Pellitteri-Hahn, M. C.; Scarlett, C. O.; Ahmad, N. Large-scale label-free comparative proteomics analysis of polo-like kinase 1 inhibition via the small-molecule inhibitor BI 6727 (Volasertib) in BRAF(V600E) mutant melanoma cells. *J. Proteome Res.* **2014**, *13*, 5041−5050.
(24) Gimenez-Cassina, A.; Danial, N. N. Regulation of mitochondrial nutrient and energy metabolism by BCL-2 family proteins. *Trends Endocrinol. Metab.* **2015**, *26*, 165−175.
(25) Yang, Q.; Zhang, Y.; Cui, H.; Chen, L.; Zhao, Y.; Lin, Y.; Zhang, M.; Xie, L. dbDEPC 3.0: the database of differentially expressed proteins in human cancer with multi-level annotation and drug indication *Database* **2018**, *2018*, DOI: 10.1093/database/bay015.
(26) Zhang, J.; Lin, A.; Powers, J.; Lam, M. P.; Lotz, C.; Liem, D.; Lau, E.; Wang, D.; Deng, N.; Korge, P.; Zong, N. C.; Cai, H.; Weiss, J.; Ping, P. Perspectives on: SGP symposium on mitochondrial physiology and medicine: mitochondrial proteome design: from molecular identity to pathophysiological regulation. *J. Gen. Physiol.* **2012**, *139*, 395−406.
(27) Nishio, T.; Kurabe, N.; Goto-Inoue, N.; Nakamura, T.; Sugimura, H.; Setou, M.; Maekawa, M. Immunohistochemical expression analysis of leucine-rich PPR-motif-containing protein (LRPPRC), a candidate colorectal cancer biomarker identified by shotgun proteomics using iTRAQ. *Clin. Chim. Acta* **2017**, *471*, 276−282.
(28) Liao, Y.; Castello, A.; Fischer, B.; Leicht, S.; Foehr, S.; Frese, C. K.; Ragan, C.; Kurscheid, S.; Pagler, E.; Yang, H.; Krijgsveld, J.; Hentze, M. W.; Preiss, T. The Cardiomyocyte RNA-Binding Proteome: Links to Intermediary Metabolism and Heart Disease. *Cell Rep.* **2016**, *16*, 1456−1469.
(29) Marchitti, S. A.; Brocker, C.; Stagos, D.; Vasiliou, V. Non-P450 aldehyde oxidizing enzymes: the aldehyde dehydrogenase superfamily. *Expert Opin. Drug Metab. Toxicol.* **2008**, *4*, 697−720.
(30) Singh, S.; Brocker, C.; Koppaka, V.; Chen, Y.; Jackson, B. C.; Matsumoto, A.; Thompson, D. C.; Vasiliou, V. Aldehyde dehydrogenases in cellular responses to oxidative/electrophilic stress. *Free Radic. Biol. Med.* **2013**, *56*, 89−101.
(31) Ghafourifar, P.; Cadenas, E. Mitochondrial nitric oxide synthase. *Trends Pharmacol. Sci.* **2005**, *26*, 190−195.
(32) Zhang, P.; Zhang, L.; Li, Y.; Zhu, S.; Zhao, M.; Ding, S.; Li, J. Quantitative Proteomic Analysis To Identify Differentially Expressed Proteins in Myocardium of Epilepsy Using iTRAQ Coupled with Nano-LC-MS/MS. *J. Proteome Res.* **2018**, *17*, 305−314.
(33) Yang, M.; Brackenbury, W. J. Membrane potential and cancer progression. *Front. Physiol.* **2013**, *4*, 185.
(34) Liu, Y.; Zhu, X.; Zhu, J.; Liao, S.; Tang, Q.; Liu, K.; Guan, X.; Zhang, J.; Feng, Z. Identification of differential expression of genes in hepatocellular carcinoma by suppression subtractive hybridization combined cDNA microarray. *Oncol. Rep.* **2007**, *18*, 943−951.
(35) Pentheroudakis, G.; Kotoula, V.; Fountzilas, E.; Kouvatseas, G.; Basdanis, G.; Xanthakis, I.; Makatsoris, T.; Charalambous, E.; Papamichael, D.; Samantas, E.; Papakostas, P.; Bafaloukos, D.; Razis, E.; Christodoulou, C.; Varthalitis, I.; Pavlidis, N.; Fountzilas, G. A study of gene expression markers for predictive significance for bevacizumab benefit in patients with metastatic colon cancer: a translational research study of the Hellenic Cooperative Oncology Group (HeCOG). *BMC Cancer* **2014**, *14*, 111.
(36) Burak, E.; Yogev, O.; Sheffer, S.; Schueler-Furman, O.; Pines, O. Evolving dual targeting of a prokaryotic protein in yeast. *Mol. Biol. Evol.* **2013**, *30*, 1563−1573.
(37) Grimsrud, P. A.; Carson, J. J.; Hebert, A. S.; Hubler, S. L.; Niemi, N. M.; Bailey, D. J.; Jochem, A.; Stapleton, D. S.; Keller, M. P.; Westphall, M. S.; Yandell, B. S.; Attie, A. D.; Coon, J. J.; Pagliarini, D. J. A quantitative map of the liver mitochondrial phosphoproteome reveals posttranslational control of ketogenesis. *Cell Metab.* **2012**, *16*, 672−683.
(38) Williamson, C. D.; Wong, D. S.; Bozidis, P.; Zhang, A.; Colberg-Poley, A. M. Isolation of Endoplasmic Reticulum, Mitochondria, and Mitochondria-Associated Membrane and Detergent Resistant Membrane Fractions from Transfected Cells and from Human Cytomegalovirus-Infected Primary Fibroblasts. *Curr. Protoc. Cell Biol.* **2015**, *68*, 3.27.1−3.27.33.
(39) Choi, Y. S.; Hoon Jeong, J.; Min, H. K.; Jung, H. J.; Hwang, D.; Lee, S. W.; Kim Pak, Y. Shot-gun proteomic analysis of mitochondrial D-loop DNA binding proteins: identification of mitochondrial histones. *Mol. Biosyst.* **2011**, *7*, 1523−1536.
(40) Lee, W. C.; Chou, H. S.; Wu, T. J.; Lee, C. F.; Hsu, P. Y.; Hsu, H. Y.; Wu, T. H.; Chan, K. M. Down-regulation of metabolic proteins in hepatocellular carcinoma with portal vein thrombosis. *Clin. Proteomics* **2017**, *14*, 29.
(41) Tohme, S.; Yazdani, H. O.; Liu, Y.; Loughran, P.; van der Windt, D. J.; Huang, H.; Simmons, R. L.; Shiva, S.; Tai, S.; Tsung, A. Hypoxia mediates mitochondrial biogenesis in hepatocellular carcinoma to promote tumor growth through HMGB1 and TLR9 interaction. *Hepatology* **2017**, *66*, 182−197.
(42) Tian, T.; Ikeda, J.; Wang, Y.; Mamat, S.; Luo, W.; Aozasa, K.; Morii, E. Role of leucine-rich pentatricopeptide repeat motif-containing protein (LRPPRC) for anti-apoptosis and tumourigenesis in cancers. *Eur. J. Cancer* **2012**, *48*, 2462−2473.
(43) Wang, L.; Morizono, H.; Lin, J.; Bell, P.; Jones, D.; McMenamin, D.; Yu, H.; Batshaw, M. L.; Wilson, J. M. Preclinical evaluation of a clinical candidate AAV8 vector for ornithine transcarbamylase (OTC) deficiency reveals functional enzyme from each persisting vector genome. *Mol. Genet. Metab.* **2012**, *105*, 203−211.
(44) Matsushita, N.; Hashimoto, E.; Tokushige, K.; Kodama, K.; Tobari, M.; Kogiso, T.; Torii, N.; Taniai, M.; Shiratori, K.; Murayama, H. Investigation of ornithine carbamoyltransferase as a biomarker of liver cirrhosis. *Intern. Med.* **2014**, *53*, 1249−1257.

(45) Chen, P.; Wang, F.; Feng, J.; Zhou, R.; Chang, Y.; Liu, J.; Zhao, Q. Co-expression network analysis identified six hub genes in association with metastasis risk and prognosis in hepatocellular carcinoma. *Oncotarget* **2017**, *8*, 48948−48958.
(46) Park, K. S.; Cho, S. Y.; Kim, H.; Paik, Y. K. Proteomic alterations of the variants of human aldehyde dehydrogenase isozymes correlate with hepatocellular carcinoma. *Int. J. Cancer* **2002**, *97*, 261−265.
(47) Jiang, Y.; Sun, A.; Zhao, Y.; Ying, W.; Sun, H.; Yang, X.; Xing, B.; Sun, W.; Ren, L.; Hu, B.; Li, C.; Zhang, L.; Qin, G.; Zhang, M.; Chen, N.; Zhang, M.; Huang, Y.; Zhou, J.; Zhao, Y.; Liu, M.; Zhu, X.; Qiu, Y.; Sun, Y.; Huang, C.; Yan, M.; Wang, M.; Liu, W.; Tian, F.; Xu, H.; Zhou, J.; Wu, Z.; Shi, T.; Zhu, W.; Qin, J.; Xie, L.; Fan, J.; Qian, X.; He, F. Chinese Human Proteome Project (CNHPP) Consortium., Proteomics identifies new therapeutic targets of early-stage hepatocellular carcinoma. *Nature* **2019**, *567*, 257−261.
(48) Grigo, K.; Wirsing, A.; Lucas, B.; Klein-Hitpass, L.; Ryffel, G. U. HNF4 alpha orchestrates a set of 14 genes to down-regulate cell proliferation in kidney cells. *Biol. Chem.* **2008**, *389*, 179−187.
(49) Zhang, Y. K.; Saupe, K. W.; Klaassen, C. D. Energy restriction does not compensate for the reduced expression of hepatic drug-processing genes in mice with aging. *Drug Metab. Dispos.* **2010**, *38*, 1122−1131.
(50) Vasiliou, V.; Pappa, A. Polymorphisms of human aldehyde dehydrogenases. Consequences for drug metabolism and disease. *Pharmacology* **2000**, *61*, 192−198.
(51) Somasundaram, V.; Nadhan, R.; Hemalatha, S. K.; Kumar Sengodan, S.; Srinivas, P. Nitric oxide and reactive oxygen species: Clues to target oxidative damage repair defective breast cancers. *Crit. Rev. Oncol. Hematol.* **2016**, *101*, 184−192.
(52) Hsieh, H. J.; Liu, C. A.; Huang, B.; Tseng, A. H.; Wang, D. L. Shear-induced endothelial mechanotransduction: the interplay between reactive oxygen species (ROS) and nitric oxide (NO) and the pathophysiological implications. *J. Biomed. Sci.* **2014**, *21*, No. 3.
(53) Matsubara, K.; Higaki, T.; Matsubara, Y.; Nawa, A. Nitric oxide and reactive oxygen species in the pathogenesis of preeclampsia. *Int. J. Mol. Sci.* **2015**, *16*, 4600−4614.
(54) Na, K.; Jeong, S. K.; Lee, M. J.; Cho, S. Y.; Kim, S. A.; Lee, M. J.; Song, S. Y.; Kim, H.; Kim, K. S.; Lee, H. W.; Paik, Y. K. Human liver carboxylesterase 1 outperforms alpha-fetoprotein as biomarker to discriminate hepatocellular carcinoma from other liver diseases in Korean patients. *Int. J. Cancer* **2013**, *133*, 408−415.

https://dx.doi.org/10.1021/acs.jproteome.9b00846
J. Proteome Res. 2020, 19, 1684−1695